Pergamon

*Int. J. Heat Mass Transfer.* Vol. 40, No. 17, pp. 4073–4084, 1997
© 1997 Elsevier Science Ltd. All rights reserved
Printed in Great Britain
0017–9310/97 $17.00+0.00

PII: S0017-9310(97)00058-6

# Numerical calculation of the effect of deposit formation on heat-exchanger efficiency

D. BOURIS and G. BERGELES

Aerodynamics Laboratory, Department of Mechanical Engineering, National Technical University of Athens, 5 Heroon Polytechniou Ave, 15700 Zografou, Athens, Greece

(*Received* 8 *August* 1996 *and in final form* 7 *February* 1997)

**Abstract**—A numerically calculated deposit was used to identify the shape of a fouled tube and an orthogonal curvilinear grid was constructed in and around the deposit. The flow and temperature field was calculated and an implicit boundary condition, accounting for the effects of turbulence, was introduced at the solid–fluid interface for the simultaneous calculation of the temperature field in the fluid and the solid. Validation is presented against experimental and numerical calculations. Finally, a reduction of 8–17% in the heat transfer rate was found to occur for a deposit corresponding to 8 h of operation in a staggered tube bundle heat-exchanger of a lignite utility boiler. Thermal resistance of the deposit was also calculated.
© 1997 Elsevier Science Ltd.

## 1. INTRODUCTION

The effects of gas-side fouling on the heat transfer efficiency of heat-exchanger tube bundles is of major importance to many industrial applications. For superheaters in lignite utility boilers the ash particles present in the flue gases deposit onto the tubes, and due to their insulating properties they have an adverse effect on the heat transfer efficiency of the heat exchanger. The purpose of the present paper is to present a numerical method that will calculate the effect of the deposit formation on the heat transfer efficiency of the tube bundle through the detailed calculation of the temperature field around the tubes as well as inside the solid deposit.

For the situation of heat exchanger tube bundles, gas side fouling alters the original shape of the tubes. The tubes are usually cylindrical in shape but fouling causes the front and sometimes the back of the tubes to be covered with deposit (Fig. 1). This results in a deformed shape of the tubes which will affect the flow field in the tube bundle but which will also affect the heat transfer through the tube wall. The part of the tube surface which is fouled lowers the overall heat transfer efficiency of the tube and of the tube bundle as a whole. The details of this effect will be studied here.

Experimental measurements in the field of heat exchanger fouling have been previously published. Kim and Kim [1] studied the deposition rate of $TiO_2$ particles from combustion gases to the surface of a circular cylinder in laminar cross-flow while Gokoglou and Santoro [2] measured vapor deposition rates to burner rig test targets in the cross stream of jets. Muller-Steinhagen *et al.* [3] also measured deposition and the effect of the operating conditions was considered. They also used several fouling models to predict their measurements and verified the asymptotic behavior of the deposit formation that is assumed by these models. Most models found in the literature and global models which do not provide detailed information regarding the deposit distribution or the effect of local flow field and surface conditions; instead they consider mean flow velocities or surface temperatures to derive a fouling resistance from the asymptotic deposit mass. Epstein [4] has evaluated quite a few of these models which consider various aspects of fouling such as fluid velocity, surface roughness, impaction, diffusion, thermophoresis, reentrainment etc.; however, the deposit distribution has not been considered.

As far as numerical work is concerned, to the authors' knowledge there have been no attempts to study the distribution of the deposit onto the tube surface and the effect of the deposit and deposit material on the flow field and heat transfer rate. Through the numerical simulation presented here the effects of the material properties of the particles and surface are considered as are the effects of the surrounding flow and temperature field. An orthogonal curvilinear numerical grid is constructed for the tube bundle and the gas phase flowing around the tubes is calculated by solving the Navier–Stokes equations using a collocated volume averaging approach with the standard k–ε model accounting for turbulence. The method for the prediction of the deposition rate has already been used to calculate the deposit formation in the heat exchanger tube bundle [5]. The shape of the calculated deposit is used to define the new tube shapes and a new grid is constructed in and around the deposits. The grid extends into the solid deposit up to the tube surfaces and thus defines both the deposit-gas and the deposit-tube interface, and a

## NOMENCLATURE

$C_\mu$, $C_1$, $C_2$ turbulence model constants
$C_p$ specific heat at constant pressure [J kg$^{-1}$ K$^{-1}$]
$C_x$, $C_y$ longitudinal and lateral spacing of tube centers in a tube bundle [m]
$d$, $d_c$ diameter and core diameter [m]
$E$ wall function constant
$F$ interpolation coefficient for solid-fluid interface
$h$ scale factor ratio for orthogonal curvilinear grid
k turbulence kinetic energy per unit mass [m$^2$ s$^{-2}$]
$k$ thermal conductivity [W m$^{-1}$ K$^{-1}$]
$K_2$ empirical coefficient expressing the strength of the deposit [m s$^{-1}$ kg$^{-1}$]
$l_\xi$, $l_\eta$ metric coefficients for orthogonal curvilinear grid
$m$, $m_d$ mass per unit area and mass deposition flux [kg m$^{-2}$ and kg m$^{-2}$ s$^{-1}$]
$P(\sigma_h/\sigma_{ht})$ function for thermal boundary layer boundary conditions
$Pr$ Prandtl number ($=C_p\mu/k$)
$Q_i$, $Q_P$, $Q'_A$ impact energy, plastic deformation energy, adhesion energy [kg m$^{-2}$ s$^{-2}$]
$Q_L$, $Q_{lift}$ elastic wave propagation energy, lift force energy [kg m$^{-2}$ s$^{-2}$]
$q''_w$ heat transfer rate [W m$^{-2}$]
$R$, $R_f$ thermal resistance, fouling resistance [K m$^2$ W$^{-1}$]
$Re$ Reynolds number ($=U_0\,d\rho/\mu$)
$S_\Phi$ source terms for Navier–Stokes equations
$T$ temperature [K or °C]
$t$ time [s]
$u$, $U_0$ axial velocity, free stream velocity [m s$^{-1}$]
$v$, $V_r$ lateral velocity, particle rebound velocity [m s$^{-1}$]
$x$, $y$ Cartesian directions
$y^+$ non-dimensional distance from wall
$Y$ Vertical distance from wall [m].

Greek symbols
$\Gamma$ diffusion coefficients [kg m$^{-1}$ s$^{-1}$]
$\varepsilon$ dissipation rate of turbulence kinetic energy per unit mass [m$^2$ s$^{-3}$]
$\kappa$ wall function constant
$\mu$, $\mu_l$, $\mu_t$ effective, fluid and turbulent dynamic viscosity [kg m$^{-1}$ s$^{-1}$]
$\xi$, $\eta$ orthogonal curvilinear coordinate directions
$\rho$ density [kg m$^{-3}$]
$\sigma$ turbulent Prandtl numbers
$\tau_{er}$, $\tau_w$ eroding shear stress and wall shear stress [kg m$^{-1}$ s$^{-2}$].

new calculation is performed so that the effect of the deposit can be evaluated.

For the evaluation of the heat transfer aspects conjugate heat transfer will be dealt with and the temperature field in the solid deposit and in the fluid flow will be solved simultaneously. Sunden [6] studied the conjugate heat transfer problem for a hollow cylinder in laminar cross flow using a finite difference for-

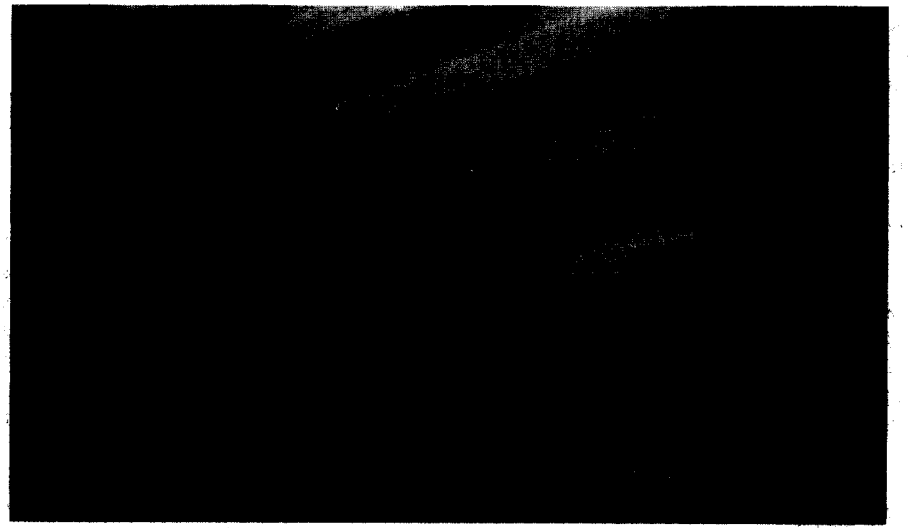

Fig. 1. Fouled tubes from the superheater of a lignite utility boiler (photo provided by the Public Power Corporation of Greece).

mulation for conservation of the heat flux at the solid–fluid interface while Patankar [7] introduced the harmonic mean for the interpolation of the thermal conductivities at the interface. In the approach presented here, the interface boundary condition that is used is implicit in the calculation procedure preserving the heat flux on either side of the interface. The effect of turbulence on heat transfer at the solid boundary is included through the wall function approach which is incorporated in the diffusion coefficient of the fluid. Validation will be presented against the results of Sunden [6] and then the method will be applied to the numerically calculated deposit formation under operating conditions that correspond to a lignite utility boiler of the Public Power Corporation of Greece. Through this calculation detailed insight will be provided on the effect of deposit formation on the temperature field and hence the heat transfer efficiency of the heat exchanger while the thermal resistance of the deposit will also be calculated.

## 2. MATHEMATICAL FORMULATION

The basic equations describing the flow field are the time averaged Navier–Stokes equations using the Boussinesq hypothesis for the calculation of the Reynolds stresses. The widely used k–ε eddy viscosity turbulence model is used to model turbulence and it involves the solution of two more equations in addition to the Reynolds equations. Thus the equations are the continuity equation, the momentum equations, the temperature (energy) equation and the two k–ε (turbulence model) equations describing the turbulence kinetic energy (k) and the turbulence energy dissipation (ε). They all reduce to a single universal form with convection and diffusion terms where a source term ($S_\Phi$) represents the other terms of each equation. It is only these source terms that differ depending on the variable. More specifically the equation expressed in orthogonal curvilinear coordinates is:

$$\frac{1}{l_\xi l_\eta}\frac{\partial}{\partial\xi}(\rho u l_\eta \Phi)+\frac{1}{l_\xi l_\eta}\frac{\partial}{\partial\eta}(\rho v l_\xi \Phi) - \frac{1}{l_\xi l_\eta}\frac{\partial}{\partial\xi}\left(\Gamma_\Phi \frac{l_\eta}{l_\xi}\frac{\partial\Phi}{\partial\xi}\right) - \frac{1}{l_\xi l_\eta}\frac{\partial}{\partial\eta}\left(\Gamma_\Phi \frac{l_\xi}{l_\eta}\frac{\partial\Phi}{\partial\eta}\right)=S_\Phi \quad (1)$$

where $(\Phi)=1$ (continuity equation), $u$ (momentum in the $\xi$ direction), $v$ (momentum in the $\eta$ direction), $T$ (temperature or $h$ enthalpy), k (turbulence kinetic energy), ε (turbulence energy dissipation). The source terms involve rather large but well known expressions in computational fluid dynamics and are not presented here due to lack of space but they can be found in Ref. [8]. Other variables are defined:

$$\mu=C_\mu\rho\frac{k^2}{\varepsilon}+\mu_l \quad \Gamma_\Phi=\frac{\mu}{\sigma_\Phi} \quad \Gamma_T=\frac{\mu-\mu_l}{\sigma_T}+\frac{\mu_l}{Pr} \quad (2)$$

where $\mu_l$ is the fluid's dynamic viscosity and $\mu$ is the effective viscosity as defined by the Boussinesq hypothesis. $Pr$ is the fluid Prandtl number and the k–ε model constants are $C_1=1.44$, $C_2=1.92$, $C_\mu=0.09$, $\sigma_{(u,v)}=1$, $\sigma_k=0.9$, $\sigma_\varepsilon=1.3$, $\sigma_T=1$.

It should be pointed out that the velocities are always defined as being parallel to the local grid lines while $l_\xi$ and $l_\eta$ are spatially varying metric coefficients related to the orthogonal curvilinear coordinates. They connect increments $d\xi$ and $d\eta$ of $\xi$ and $\eta$ in transformed space to increments of physical distance $\Delta\xi$ and $\Delta\eta$ as $\Delta\xi=l_\xi d\xi$ and $\Delta\eta=l_\eta d\eta$.

The calculation of the curvilinear orthogonal grid is achieved through the solution of the Laplace equations:

$$\frac{\partial^2 x}{\partial\xi^2}+\frac{1}{h^2}\frac{\partial^2 x}{\partial\eta^2}=0, \quad \frac{\partial^2 y}{\partial\xi^2}+\frac{1}{h^2}\frac{\partial^2 y}{\partial\eta^2}=0 \quad (3)$$

where $h$ is the ratio of the scale factors associated with the orthogonal curvilinear coordinates $\xi$ and $\eta$. More details on the grid calculation procedure can be found in Theodoropoulos *et al.* [9].

The solution procedure for equations (1) involves volume averaging and pressure correction according to the SIMPLE algorithm [10]. More details on the calculation procedure can be found in Mouzakis and Bergeles [8] who had a staggered arrangement of the variables on the grid. The exception in the present case is that variables are collocated on the grid and the Rhie and Chow [11] interpolations are used for the cell face velocities in the pressure equation. Boundary conditions are Neumann conditions at symmetry planes and wall functions at the walls.

For the simultaneous solution of the temperature field in materials of different physical properties the only point which requires extra care is the boundary between the two materials. In the situation to be examined here this is the boundary between the solid deposit and the gas flow. While the momentum and continuity equations are only solved in the region of the fluid flow, the temperature equation is solved inside the solid deposit as well. Temperature variables are stored at the centers of the computational grid cells as are the other variables (Fig. 2). However, the

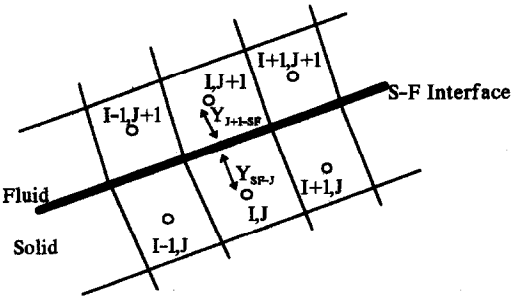


Fig. 2. Computational grid at the solid–fluid interface.

temperature at the solid fluid interface S–F is not given but must be interpolated from the neighboring values at $(I, J)$ and $(I, J+1)$. The temperature on the boundary is given through an interpolation coefficient $F$:

$$T_{S-F} = T(I,J)(1-F) + T(I,J+1)F. \tag{4}$$

The interpolation coefficient $F$ can be determined through the heat flux conservation over S–F after volume averaging and taking into account the local variation of the diffusion coefficients.

$$F = \frac{\Gamma(I,J+1)C_P(I,J+1)/Y_{J+1-SF}}{\Gamma(I,J)C_p(I,J)/Y_{SF-J} + \Gamma(I,J+1)C_p(I,J+1)/Y_{J+1-SF}} \tag{5}$$

$\Gamma(I, J)$ define the diffusion coefficients at each computational cell while $Y$ defines the distance from the S–F interface. When the cell center on the side of the fluid is in the laminar flow region then the diffusion coefficient is defined:

$$\Gamma = \frac{\mu_l}{Pr} = \frac{k}{C_P} \tag{6}$$

where $k$ is the thermal conductivity and $C_P$ is the specific heat at constant pressure. However, when the cell center is in the turbulent flow region the fluid passing over the solid boundary is subject to boundary conditions for turbulent flow involving wall functions. These wall functions define the temperature gradient at the wall for values of $y^+ > 11.63$ where $y^+ = Y\rho(\tau_w/\rho)^{0.5}/\mu_l$ and a log law of the wall gradient is calculated instead of the linear one that applies for laminar flow. This is incorporated into the interpolation procedure if equation (5) is modified by replacing the term related to the gradient above the wall with the one given by the wall function analysis, e.g.:

$$\Gamma(I,J+1)C_P(I,J+1)/Y_{J+1-SF} = \frac{C_P(I,J+1)\sqrt{K(I,J+1)}C_\mu^{0.25}\rho(I,J+1)}{\sigma_{ht}\left[\frac{1}{\kappa}\ln(Ey^+) + P\left(\frac{\sigma_h}{\sigma_{ht}}\right)\right]} \tag{7}$$

where $K(I, J+1)$ is the turbulent kinetic energy, $C_\mu = 0.09$, $E = 9.793$ and $\kappa = 0.4187$ are turbulence model constants, $\rho$ is the fluid density, $y^+$ is the non dimensional distance from the wall, $\sigma_h$ and $\sigma_{ht}$ are the laminar and turbulent Prandtl numbers and $P(\sigma_h/\sigma_{ht})$ is the $P$ function derived from experimental data for equilibrium flow over smooth surfaces [12]. This completes the definition of the interpolation that should be used for $T_{SF}$ in the diffusion terms so that the boundary condition is conservative in regard to the heat flux.

The advantages of the above mentioned boundary condition are obvious if one considers that the consistency of heat flux is implicit in the interpolation and that this will still hold even for locally varying diffusion coefficients such as those that arise from turbulence effects on the gas flow [see equation (7)]. Furthermore, the form of the interpolation allows the application of the boundary condition to the tridiagonal form of the solution procedure.

For the calculation of the particle trajectories in the flow and their impact onto the tube surfaces which will lead to their rebound or adhesion to the surface a Lagrangian particle tracking method [13] and a deposition model [5] were employed. The Lagrangian particle tracking method considers the anisotropy of the turbulence through an algebraic Reynolds stress model and determines the position and velocity of impact to the tube surface. The adhesion or rebound of the particles is determined by an energy balance at the point of impact, taking into account the material properties of the particle and surface to calculate the elastic and plastic deformations while the surface energy is used to determine the forces holding the particle to the surface. Thus the particle rebound velocity is given by:

$$V_r = \left[\frac{2}{m_P}(Q_i - Q_P - Q'_A - Q_L + Q_{lift})\right]^{(1/2)} \tag{8}$$

where $m_P$ is the particle mass. The initial kinetic energy of the particle at impact $Q_i$ is lost to plastic deformation energy $Q_P$ and dissipated as energy due to elastic wave propagation $Q_L$ (from Reed [23]). The remaining energy (stored as elastic energy) is then returned to the particle and if it is larger than the energy due to attractive forces between particle and surface $Q'_A$ then the particle will rebound, otherwise it will stick to the surface. The attractive forces are mostly due to van der Waals–London dispersion forces, [4]. $Q_{lift}$ is the aerodynamic lift energy that is gained by the particle due to hydrodynamic lift forces (Saffman lift force).

The expressions of these energy terms are quite complex and for a particle of known size and velocity they are functions of material properties of the particle and the surface to which it impacts: Young's modulus, Poisson's ratio, elastic yield limit of the softer of the two materials, particle density and interfacial surface energy derived from the dispersive surface energies of the two materials, [14]. These expressions, used by Wall *et al.* [15] were originally introduced by Bitter [16] based on the Hertz theory. The expression for the lift energy near the wall is based on the Saffman lift force according to an analysis by Hall [17] and can be found in Ref. [5].

The evolution of the deposit in time considers the fluid shear stress as well as the shearing of the deposit by the tangential particle impacts, and the deposited mass per unit area as a function of time is given by:

$$m = \frac{m_d^*}{K_2(\tau_w + \tau_{er})}\{1 - \exp[-K_2(\tau_w + \tau_{er})t]\} \tag{9}$$

where $m_d^*$ is the depositing mass flux, $\tau_w$ and $\tau_{er}$ are the fluid shear stress and the eroding shear stress, $t$ is time and $K_2$ is a constant related to the strength of the

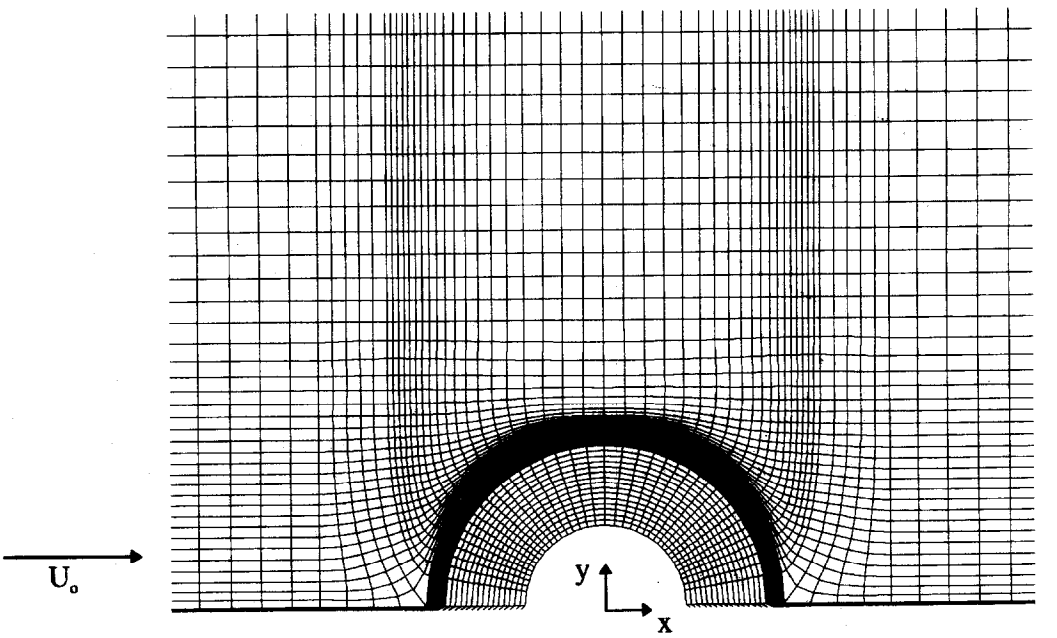


Fig. 3. Close up of orthogonal curvilinear and polar grid used for the calculations (122 × 116).

deposit. More details on the particle deposition model can be found in Bouris and Bergeles [5].

## 3. VALIDATION OF THE NUMERICAL APPROACH

The numerical code has been used for the prediction of laminar and turbulent cross flow past cylinders. The laminar flow field calculation is compared to the experimental measurements of Coutenceau and Bouard [18] for the velocity on the centerline behind a circular cylinder in laminar cross flow. Heat transfer validation is presented with the computational results of Sunden [6]. The configuration is of a circular hollow cylinder with a core of constant temperature and laminar cross flow across the outer side. The core has a diameter $d_c = 0.5d$ where $d$ is the outer diameter of the cylinder.

A close up of the orthogonal curvilinear grid used in all the calculations is presented in Fig. 3. The grid is a combination of a standard orthogonal curvilinear grid further away from the cylinder outer surface and a polar grid for the cylinder wall which extends another 10% of the cylinder diameter from the cylinder surface. The polar grid was necessary for the cylinder wall and the extension from the cylinder surface was warranted to push away the grid discontinuity that always exists at the stagnation point for orthogonal curvilinear grids around cylinders. The grid extends $16.6d$ above the symmetry axis of the cylinder and $5.5d$ and $11d$ before and after the cylinder center, respectively, and is $122 \times 116$ in size.

The predictions of the centerline axial velocity behind the cylinder are in good agreement with the experimental measurements (Fig. 4). For the conjugate heat transfer situation calculations were made for various thermal conductivities of the solid material of the cylinder. Sunden's [6] calculations were performed on a transformed grid system using the finite difference approach and the relaxation method. The boundary condition at the solid-fluid interface was also determined by the heat flux and temperature consistency criteria. The fact that the present finite volume approach on a collocated grid system with the SIMPLE pressure correction method yields practically the same results is reassuring as to the correct behavior of the method in heat transfer predictions (Fig. 5). Finally, prediction of turbulent heat transfer on a circular cylinder in cross flow at a higher Reynolds number ($Re = 10\,000$) is compared against experimental measurements of Perkins and Leppert [19] (Fig. 6). This value of the Reynolds number, although not fully turbulent according to theory, is

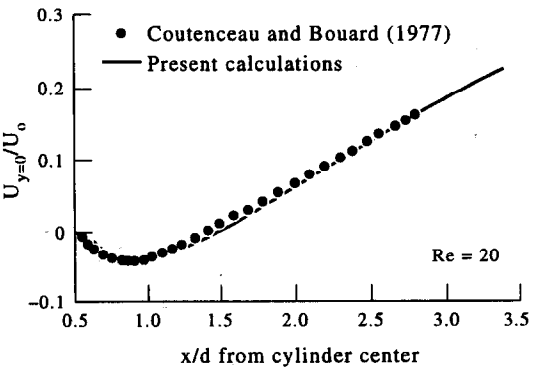


Fig. 4. Predictions of axial velocity on centreline behind a cylinder in laminar cross-flow.

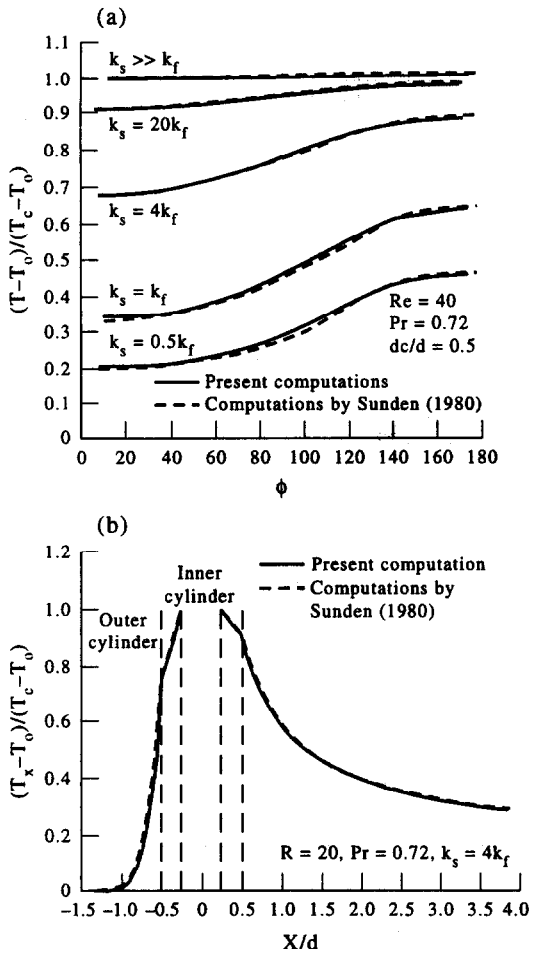


Fig. 5. Numerical calculation of conjugate heat transfer from a hollow cylinder in laminar cross flow. (a) Non-dimensional surface temperature distribution ($T_c$ is core temperature and $T_0$ free stream temperature) for various solid–fluid conductivity ratios; (b) non-dimensional temperature on symmetry axis of cylinder ($x/d = 0$ is the cylinder center).

very close to the values that we see in heat exchanger tube bundles and is therefore representative for the heat transfer calculations that will be presented for a staggered tube bundle in another part of this paper. The results for the turbulent calculation are considered acceptable given the uncertainty regarding the fully turbulent nature of the boundary layer which at this Reynolds number should develop laminar at the front of the cylinder to become turbulent at separation. The effect of this transition is carried downstream after separation.

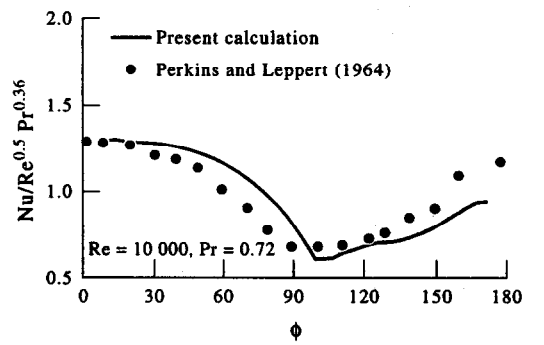


Fig. 6. Predictions of Nusselt number distribution on the surface of a cylinder in cross-flow at $Re = 10\,000$.

## 4. APPLICATION TO HEAT EXCHANGER FOULING

For a staggered tube bundle arrangement with clean tubes at a longitudinal spacing of $C_x/d = 1.6$ and a transverse spacing of $C_y/d = 3.6$ the calculation of the flow field and comparison with experimental measurements have already been presented in Refs [5] and [20]. Using the particle deposition model briefly described in equations (8) and (9) the deposit formation on the same tube bundle under industrial operating conditions for both flow and particles (as provided by the Public Power Corporation of Greece) was calculated. The calculation assumed a mass loading of 1% and a diameter distribution involving four particle diameters from 45 to 700 $\mu$m with material properties corresponding to $Al_2O_3$. More details can be found in Ref. [5]. The shape of the calculated deposits corresponding to 8 h of operation led to the construction of a new tube bundle with the same configuration, but with deformed tubes according to the shape indicated by the deposit. Experimental measurements were performed in the tube bundle by King's College London [21]. A new orthogonal curvilinear grid was now constructed to fit the deformed shape of the tubes while it was also extended inside the solid deposits so that they may be included in the calculation domain. The grid is presented in Fig. 7 where the bottom half shows the grid domain used for the momentum and continuity equations, while the top half shows the full grid used for the temperature calculation. It should be noted that in order to construct a grid in such a complex domain the grid around the deposits was constructed first and then the distribution of the grid lines on the surfaces of the deposits determined the one boundary of the almost triangular-shaped deposits. The grids inside the deposits were then constructed in order to match the outer grid, but it was necessary for a given number of grid lines to extend under the symmetry boundary as well as into the cylinder area. These lines are, of course, not included in the solution procedure and therefore their position or distribution has no influence. Streamlines in the tube bundle with deformed tubes are presented in Fig. 8 and comparison with experimental measurements are presented in Fig. 9 for a Reynolds number of $Re_d = 12\,858$. The calculation domain extends well beyond the experimentally measured domain, so that the length of the recirculation zones will not affect the prediction in the area of the outlet.

A deposit that forms on the surface of the tubes of the heat-exchanger tube bundle would inevitably

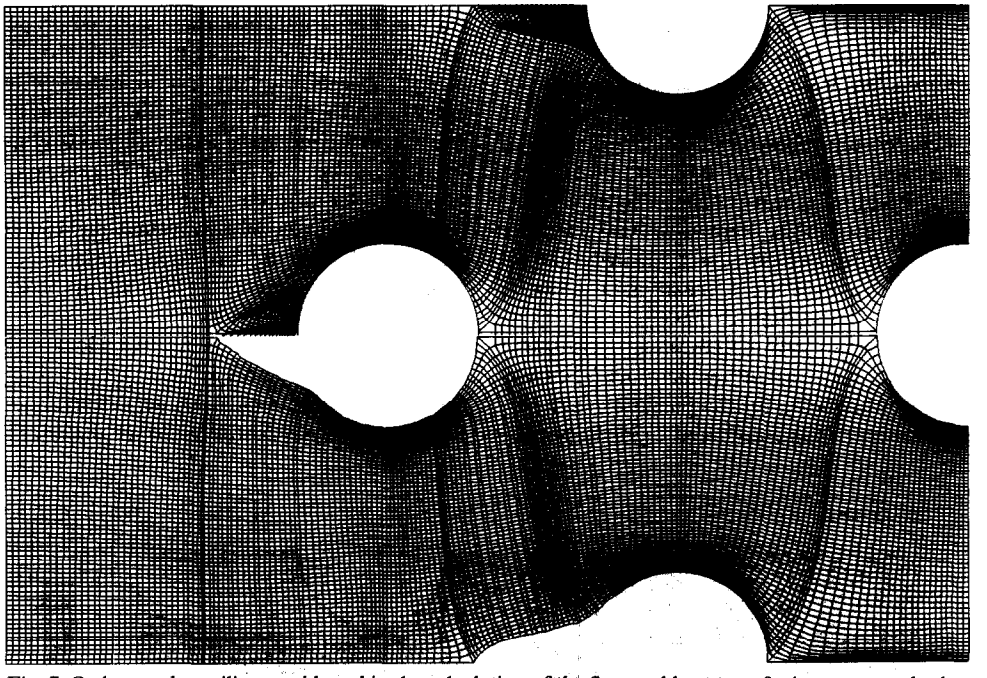

Fig. 7. Orthogonal curvilinear grid used in the calculation of the flow and heat transfer in a staggered tube bundle with deposit formation on two of the tubes. The grid is $178 \times 113$, grid spacing $C_x/d = 1.6$, $C_y/d = 3.6$.

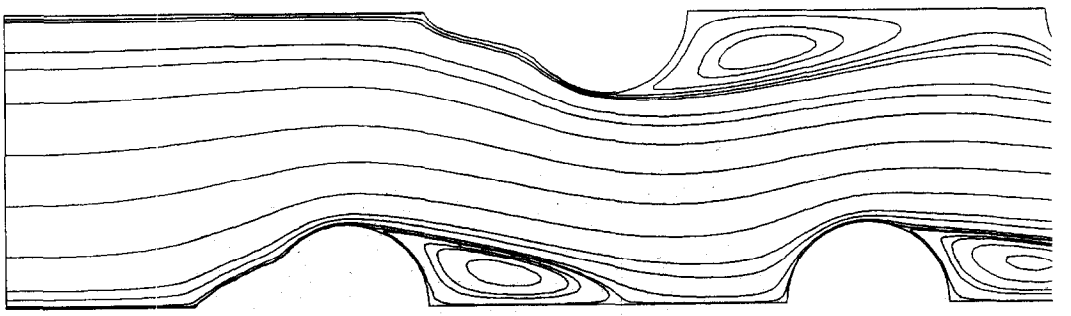

Fig. 8. Streamlines in staggered tube bundle with fouled tubes: $Re = 12858$.

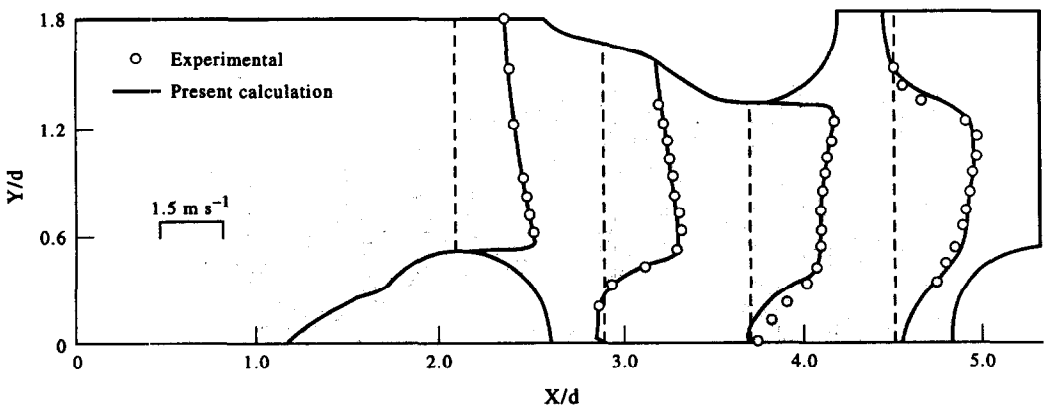


Fig. 9. Numerical predictions of mean $U$ axial velocity measurements in staggered tube bundle with fouled tubes: $Re = 12858$.

affect both the flow field and the heat transfer efficiency of the tube bundle. The main effects on the flow field are slightly shorter recirculation zones and higher turbulence levels, while the flow velocity in the passage between the tubes increases. The impact of these differences will be discussed later. In order to identify the effect on the heat-transfer efficiency industrial operating conditions were used and the heat transfer at the tube surfaces was evaluated. The air properties at the inlet were mean axial velocity $U_0 = 12$ m s$^{-1}$ and temperature 900°C. The tube surfaces were assumed to have a constant temperature of 600°C. Although the constant temperature boundary condition is questionable, for the purpose of the present investigation it was considered a good approximation. For the deposit, exact thermal properties are not well defined and an initial assumption would be to use those of the most prominent material in the deposit which is $Al_2O_3$ [21]. However, this is a metal oxide with a conductive nature ($k = 7.0$ W m$^{-1}$ K$^{-1}$, $C_P = 245$ J kg$^{-1}$ K$^{-1}$) and for this reason another substance was also considered to better simulate the insulating behavior of the ceramic like deposit (sandstone $k = 1.73$ W m$^{-1}$ K$^{-1}$, $C_P = 711$ J kg$^{-1}$ K$^{-1}$). Muller-Steinhagen *et al.* [3] found $k$ of the order 1 W m$^{-1}$ K$^{-1}$ for kaolin deposits.

In Figure 10 the temperature field for the clean tubes, the fouled tubes with $Al_2O_3$ deposit and the fouled tubes with Sandstone deposit are shown. The tube numbering is according to the distance from the

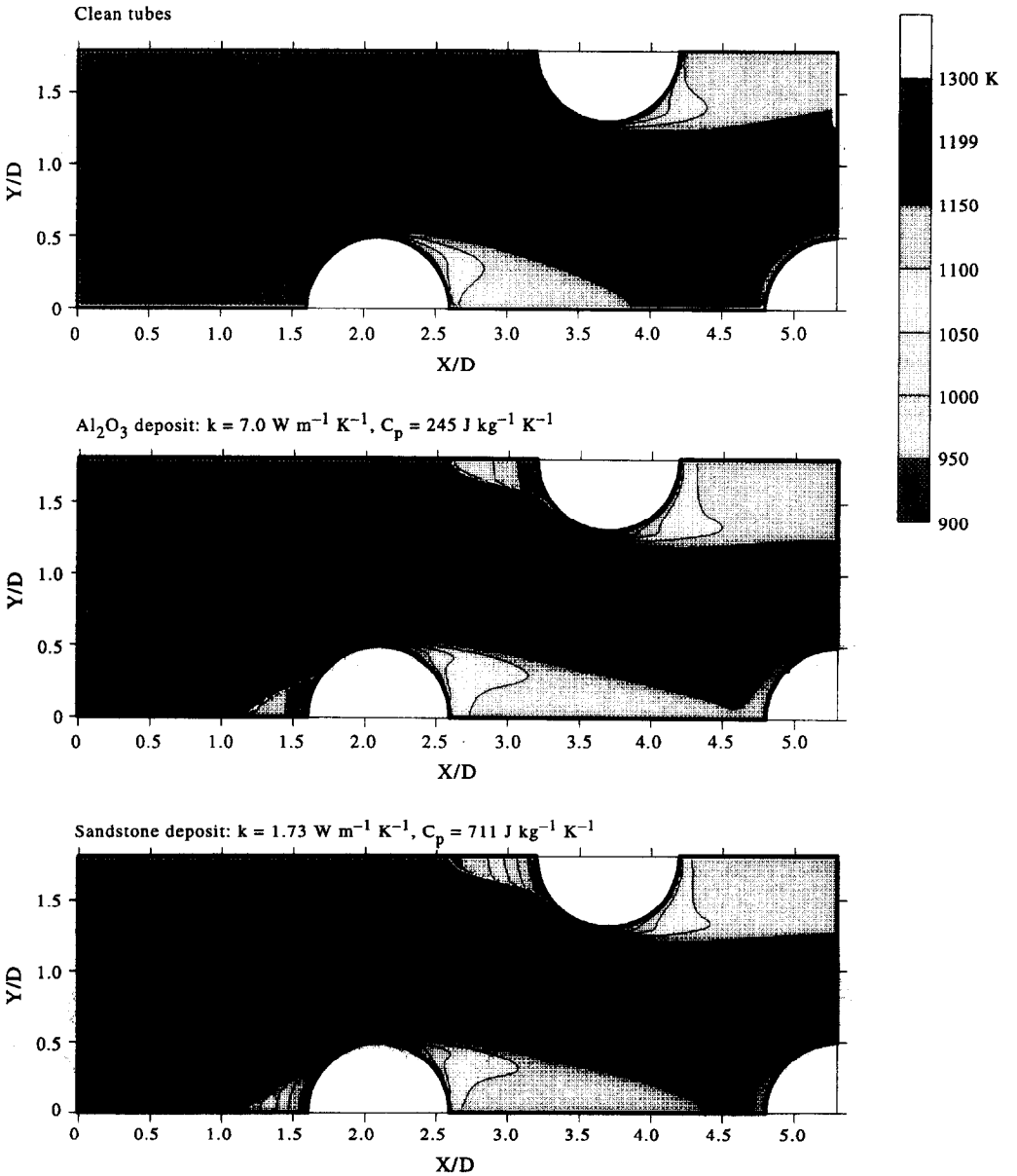


Fig. 10. Temperature fields in staggered tube bundle with clean and fouled tubes. Industrial operating conditions $Re \sim 3000$. The gas temperature is 900°C and the tube wall temperature 600°C.

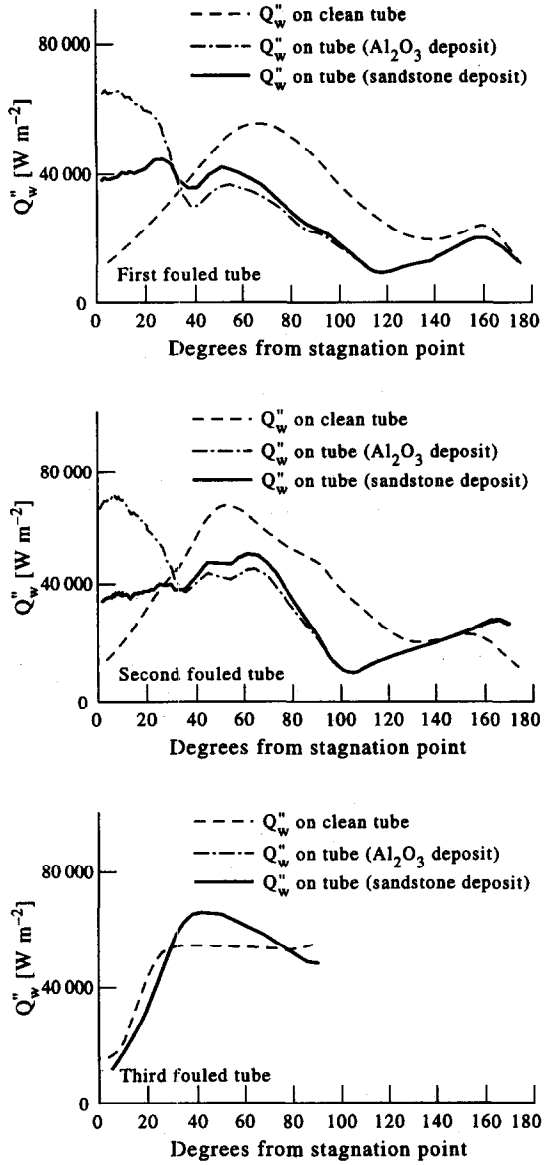


Fig. 11. Numerical calculation of heat transfer rate to tube surfaces for clean and fouled tubes and for two different deposit materials. Same conditions as in Fig. 10.

inlet (first and third tube are on the bottom). In Fig. 11 the heat transfer rate to the tube surfaces are plotted per tube surface area for the three tubes for the same three situations. The alternative plotting of a Nusselt number distribution would not be representative in this situation due to the difference in thermal conductivity between the solid and the fluid along the tube surface.

An interesting phenomenon is observed in the fouled region of the first two tubes (Fig. 11). The convective heat transfer from the fluid to the deposit surface area is directed through conduction to the small corresponding area of the tube surface (0–40° region) and the result is a local increase in the heat transfer rate to the tube. However, the insulating properties of the deposit work against this and the increase in heat transfer cannot be explained by the area difference alone. This is evident from the difference in the heat transfer rates for the $Al_2O_3$ and the sandstone deposit. The more insulating sandstone material causes larger temperature gradients in the deposit and therefore higher deposit surface temperatures and lower heat transfer rates than $Al_2O_3$. In both cases, though, the increased surface area still keeps the level higher than the clean tube.

The overall heat transfer rate per tube is reduced, as would be expected, but it is interesting to note the effect of the fouled region on the rest of the tube. For both deposit materials, in the region after the deposit, the heat transfer rate is lower than for the clean tube, but the $Al_2O_3$ deposit is the lower of the two. The smaller temperature gradients in the $Al_2O_3$ (higher thermal conductivity) lead to lower deposit surface temperatures, which benefit heat transfer. However, the temperature gradient of the deposit is carried downstream for a short distance where it comes into contact with the wall temperature at the clean tube surface (40–180°) and it lowers the heat transfer rates there (Fig. 11). The variation in the temperature gradient is shown for the top of the first tube in Fig. 12. From the overall form of the temperature boundary layer in Fig. 9 it is evident that the higher fluid velocities in the passage lead to a thinner temperature boundary layer separating from the fouled tube while the deposit temperature gradient mainly influences the tube surfaces region and the area between the first and third tube. For the conductive $Al_2O_3$ the smaller temperature gradient causes the temperatures between the first and third tube and in the recirculation zone to be lower and they are carried closer to the surface of the third tube.

The third tube shows a different behavior, since at this stage there is no deposit formed on its surface. Although the temperature gradient in the deposit leads to lower temperatures between the first and third

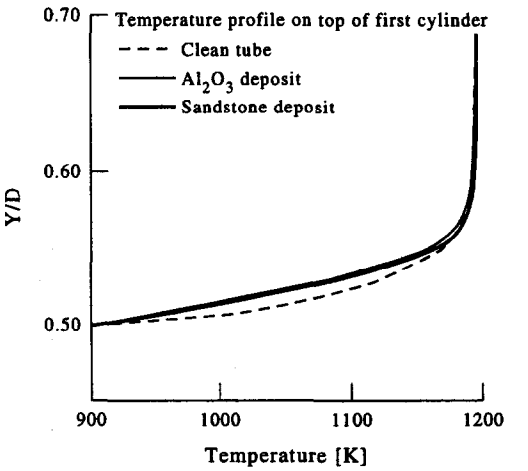


Fig. 12. Temperature profile at top of first tube for the three situations of Fig. 10.

Table 1. Average heat flux and thermal resistance for the clean and fouled tubes in a staggered arrangement tube bundle

| | $q''_w$ (kW m$^{-2}$) | | | $R$ (K m$^2$ W$^{-1}$) | | | $R_f$ (K m$^2$ W$^{-1}$) | |
|---|---|---|---|---|---|---|---|---|
| | Clean | $Al_2O_3$ | Sandstone | Clean | $Al_2O_3$ | Sandstone | $Al_2O_3$ | Sandstone |
| 1st tube | 31.2 | 27.7 | 25.8 | 0.0096 | 0.0108 | 0.0116 | 0.0012 | 0.002 |
| 2nd tube | 36.2 | 33.3 | 30.6 | 0.0083 | 0.009 | 0.0098 | 0.0007 | 0.0015 |
| 3rd tube | 47.3 | 48.6 | 49.1 | | | | | |
| Total | 114.7 | 109.6 | 105.5 | | | | | |

tube the thinner temperature boundary layer that separates from the first tube and reaches the top of the third leads to a larger temperature gradient there. This results in lower heat transfer rates at the front of the third tube, but there is a substantial increase at the top (Fig. 11). Only the first half of the tube is presented since the calculation domain for the clean tubes was confined to this area. Overall, the increase in the heat transfer rates on the third tube might be an indication towards the use of easily replaceable or cleanable tubes for the first rows of heat exchangers. They would be the most prone to fouling and if they do not participate in the heat transfer process they would act as filters while allowing the transfer of heat to the subsequent rows and maintaining the heat transfer rates.

The next step is to calculate the average heat flux on the tubes and to find the overall effect of the deposit formation on the heat transfer rates. The fouling resistance of the deposits will also be calculated from the thermal resistance of the clean and fouled tubes. The thermal resistance is defined:

$$R = \frac{\Delta T}{q''_w} \tag{10}$$

where $\Delta T$ is the temperature difference between the wall and the upstream flow and $q''_w$ is the average heat transfer rate on the tube. The results for the thermal resistances and heat transfer rates are presented in Table 1. The average values are calculated from the sum of the heat transfer rates at each cell face on the tube wall divided by the total area of the cell faces.

The average heat flux on the third tube is only indicative since only the first half of the clean tube was used for the calculation and the back of the tube where heat transfer is usually reduced would have brought down the calculated average value. In any case the presence of the deposit on the first two tubes gives the heat flux on the third tube an increase of about 3–4% depending on the material of the deposit. For the first tube, however, we have an overall reduction of 11–17% in the heat transfer and for the second tube we have a reduction of 8–15% again depending on the material of the deposit. The values of the fouling resistances are in agreement with the asymptotic fouling resistances that Muller-Steinhagen *et al.* [3] measured for $Al_2O_3$ depositing from heptane onto an annular probe. Their values were in the range $R_f = 0.5\text{–}5 \times 10^{-3}$ Km$^2$ W$^{-1}$. For the total heat transfer of the first 2.5 rows of the tube bundle it was found that the presence of the deposit leads to a 4.5% reduction for the $Al_2O_3$ deposit and an 8% reduction for sandstone.

Having calculated the effect on the heat transfer rate up to the first 8 h of operation, another deposition rate could be calculated for the new tube shapes in order to investigate the effect of the deposit formation. If calculations are continued in this fashion until asymptotic deposit formation is reached the effect would be more pronounced and deposits would have been formed at other points of the tube bundle as well. Such a computation has been performed by Bouris and Bergeles [5]. The extension of the 8 h calculation presented here leads to an asymptotic deposit in just over 10 days.

Rugge and Bohnet [22] have performed experimental studies of fouling in staggered tube bundles. The tube bundle they studied had a spacing of $C_x/d = 286$, $C_y/d = 1.8$ and the flow, at a Reynolds number of 29 000 was seeded with PVC particles of 40 $\mu$m diameter. The conditions are obviously different from the ones studied here in that the lateral spacing is half the one studied here and this is expected to result in much faster fouling rates. However, with the difference in operating conditions kept in mind, certain comparisons can be made. As expected, Rugge and Bohnet [22] found the asymptotic state to be reached in only 2 h. The deposit thickness measured by Rugge and Bohnet [22] on the second row is found larger than on the first row while the third row shows minimal deposit formation. This behaviour of the deposit formation is also observed in the present calculation. Rugge and Bohnet [22] also measured the variation of heat flux through the cylinder wall with deposit formation. It was found that the heat flux has fallen to 50% of its initial value within 30 min (25% of the time to asymptotic state). Of course, a direct comparison cannot be made since the thermal properties of the deposit play an important role as well as the fact that the temperature on the tube wall is determined in the experiments by the fluid flowing inside the tube. This is a different boundary condition from the constant temperature applied here. However, the predicted drop in heat transfer to the first row by 8–17% in the first 8 h of operation (3.5% of the asymptotic time) is reasonable when compared to the measured drop of 50% in 25% of the asymptotic time.

Ideally there should be more computations per-

formed at regular intervals so that the effect of the deposit on the flow field and the heat transfer rate can be given as a function of time. This is a very tedious task considering the fact that a new grid must be reconstructed in and around the new deposit at every time interval. The authors are currently investigating a novel boundary condition that will allow the definition of a solid–fluid interface in such a way that it will not necessarily coincide with a grid line (porosity technique), thus permitting recalculation without reconstruction of the grid.

## 5. CONCLUSIONS

A numerical model is presented for the calculation of the effect of deposit formation on heat transfer rates in heat exchanger tube bundles. The model takes into account the thermal properties of the deposit material. A heat transfer consistency boundary condition is used at the solid–fluid interface so the computational domain extends through the solid deposit up to the tube surface. The boundary condition is implicit in the numerical procedure and takes into account the effects of turbulence on the heat transfer rate at the surface using wall functions for the local variation of diffusion coefficients. The numerical model was validated against previously published experimental and numerical results for laminar and turbulent flow and heat transfer past a circular cylinder. Conjugate heat transfer was also calculated for a hollow cylinder with a constant temperature core.

After validation, the model was used to calculate the effect of deposit formation on a superheater in a lignite utility boiler. The deposit corresponds to 8 h of industrial operating conditions and was numerically calculated. This deposit defines a new shape for the tubes so the flow and temperature field was recalculated for two different types of deposit material. The presence of the insulating deposit leads to a thinner temperature boundary layer separating from the top of the fouled tubes but lower temperatures are observed in the recirculation region behind the tubes. This is mainly influenced by the temperature gradient present in the deposit and results in an overall reduction for the heat transfer rates on the fouled tubes and an increase for the tube in the third row. The heat transfer efficiency of the heat exchanger was calculated and the thermal resistances of the clean and fouled tubes were used to calculate the fouling resistance of the deposit. It was found that the deposit formation leads to an 8–17% reduction in the heat transfer rate to the fouled tubes depending on the position of the tube and the thermal properties of the deposit material. The overall effect on the tube bundle is a reduction by about 4–8% since the tube in the third row actually shows signs of an increase in the heat transfer rate.

An interesting observation is the complexity of the temperature boundary layer separating from the fouled tubes. The smaller temperature gradient of the deposit influences the region near the fouled tube surface and in the recirculation zone, but the increase in fluid velocity in the tube bundle passages results in a thinner layer that reaches the tube in the third row and increases the local heat transfer rate there. The overall increase in the heat transfer rate on the third tube can be considered as an indication for the use of tubes that do not participate in the heat transfer process for the first few rows where fouling is most pronounced, and thus heat transfer may be allowed to be recovered at the subsequent rows.

*Acknowledgements*—The work presented in this paper was funded in part by the Commission of the European Communities under the JOULE II Program, contract number JOU2-CT92-0014. Collaborating partners were the National Technical University of Athens, King's College London and the Public Power corporation of Greece.

## REFERENCES

1. Kim, Y. J. and Kim, S. S., Experimental study of particle deposition onto a circular cylinder in high-temperature particle laden flows. *Experimental Thermal and Fluid Sciences*, 1992, **5**, 116–123.
2. Gokoglou S. A. and Santoro, G. J., Determination of convective diffusion heat/mass transfer rates to burner rig test targets comparable in size to cross-stream jet diameter. *Journal of Heat Transfer*, 1988, **110**, 449–455.
3. Muller-Steinhagen, H., Reif, F., Epstein, N. and Watkinson, A., Influence of operating conditions on particulate fouling. *Canadian Journal of Chemical Engineering*, 1988, **66**, 42–50.
4. Epstein, N., Particulate fouling of heat transfer surfaces: mechanisms and models. In *Fouling Science and Technology*, ed. L. F. Melo, T. R. Bott and C. A. Bernardo. Kluwer Academic, Dordrecht, 1988, pp. 143–164.
5. Bouris, D. and Bergeles, G., Particle-surface interactions in heat exchanger fouling. *Journal of Fluids Engineering*, 1996, **118**, pp. 574–581.
6. Sunden, B., Conjugated heat transfer from circular cylinders in low Reynolds number flow. *International Journal of Heat & Mass Transfer*, 1980, **23**, 1359–1367.
7. Patankar, S. V., *Numerical Heat Transfer and Fluid Flow*, ed. W. Minkowycz and E. Sparrow. Hemisphere, Washington, DC, 1980.
8. Mouzakis, F. and Bergeles, G., Numerical prediction of turbulent flow over a two dimensional ridge. *International Journal of Numerical Methods in Fluids*, 1991, **12**, 287–296.
9. Theodoropoulos, T., Bergeles, G. and Athanasiadis, N., Orthogonal grid generation in two dimensional space. *Proceedings of the 4th International Conference on Numerical Methods in Laminar and Turbulent Flow*, 1985, pp. 1747–1758.
10. Patankar, S. V. and Spalding D. B., A calculation procedure for heat, mass and momentum transfer in three dimensional parabolic flows. *International Journal of Heat and Mass Transfer*, 1972, **15**, 1787.
11. Rhie, C. and Chow, W., Numerical study of the turbulent flow past an airfoil with trailing edge separation. *AIAA Journal*, 1985, **21**, 1525–1532.
12. Spalding, D. B., Contribution to the theory of heat transfer across a turbulent boundary layer. *International Journal of Heat & Mass Transfer*, 1964, **7**, 743–761.
13. Burry, D. and Bergeles G., Dispersion of particles in anisotropic turbulent flows. *International Journal of Multiphase Flow*, 1993, **19**, 651–664.

14. Fowkes, F., Attractive forces at interfaces. *Industrial and Engineering Chemistry*, 1984, **56,** 12, 40–52.
15. Wall, S., John, W. and Goren, S., Application of impact adhesion theory to particle kinetic energy loss measurements. In *Particles on Surfaces* 2, ed. K. L. Mittal. Plenum Press, New York, 1988.
16. Bitter, J., A study of erosion phenomena (part I). *Wear*, 1963, **6,** 5–21.
17. Hall, D., Measurements of the mean force on a particle near a boundary in turbulent flow. *Journal of Fluid Mechanics*, 1988, ***187,*** 451–466.
18. Coutenceau M. and Bouard, R., Experimental determination of the main features of the viscous flow in the wake of a circular cylinder in uniform translation. Part 1. Steady flow. *Journal of Fluid Mechanics*, 1977, **79,** 231–256.
19. Perkins, H. C. and Leppert, G., Local heat transfer coefficients on a uniformly heated cylinder. *International Journal of Heat Mass Transfer*, 1964, **7,** 143–158.
20. Balabani, S., Bergeles, G., Burry, D. and Yianneskis, M., Velocity characteristics of the crossflow over tube bundles. *Proceedings of the 7th International Symposium on Applications of Laser Anemometry to Fluid Mechanics*, Vol. II, Lisbon, 1994, pp. 39.3.1–39.3.8.
21. Bergeles, G., Bouris-Burry, D., Yianneskis, M., Balabani, S., Kravaritis, A. and Itskos, S., Effects of fouling on the efficiency of heat exchangers in lignite utility boilers. Final Report, Joule II Programme Contract No. JOU2-CT92-0014, 1996.
22. Rugge, J. and Bohnet, M., Wissenschaftliche Forschungsarbeit. *Chemie-Ingenieur-Technik*, 1991, **63,** 1144–1145.
23. Reed, J., Energy losses due to elastic wave propagation during an elastic impact. *Journal of Physics D*, 1985, **18,** 2329–2337.